Intermolecular Interactions between Cholecystokinin-8 and the Third Extracellular Loop of the Cholecystokinin-2 Receptor[†,‡]

Craig Giragossian[§] and Dale F. Mierke*[,§,||]

Departments of Chemistry and Molecular Pharmacology, Division of Biology and Medicine, Brown University, Providence, Rhode Island 02912

Received December 3, 2001; Revised Manuscript Received February 11, 2002

ABSTRACT: The structure of the third extracellular loop of the human cholecystokinin-2 receptor, CCK_2-R(352−379), and its interactions with the C-terminal octapeptide of cholecystokinin (CCK-8) have been determined by high-resolution NMR and computer simulations. In the presence of dodecylphosphocholine micelles, the structure of the receptor fragment consisted of three helices, with the first and third corresponding to residues of the extracellular ends of transmembrane helices (TM) 6 and 7, respectively. The central, extracellular helix, consisting of residues 363−368, was found to be closely associated with the membrane mimetic used during the spectroscopic studies and molecular dynamics (MD) simulations. Upon titration of CCK-8 to the receptor domain, chemical shift perturbation and intermolecular NOEs (Trp^{30}, Met^{31} of CCK-8 and P371, F374 of CCK_2-R) indicated the formation of a stable complex and specific ligand/receptor interactions. Using the NOE-generated intermolecular contact points, extensive MD simulations of CCK-8 bound to the CCK_2 receptor were carried out. The results, with CCK-8 in close proximity to TM7, differ from previous structural studies of CCK-8 association with CCK_1-R, in which the ligand formed a number of interactions with TM6. These differences may play a role in the ligand specificity displayed by the CCK_1 and CCK_2 receptor subtypes.

The cholecystokinin-2 receptor (CCK_2-R)[1] is a member of the rhodopsin class (class A) of G-protein-coupled receptors (GPCR) that are structurally characterized by seven membrane-spanning domains, an extracellular N-terminus, and an intracellular C-terminus. The receptor plays a role in the regulation of multiple physiological functions in the central nervous system (e.g., anxiety, satiety, analgesia, and memory) and in the gastrointestinal tract (e.g., gastric acid secretion and mucosal and enterochromaffin-like cell proliferation in the gastric epithelium) (*1*−*6*). In addition to a role as a growth factor for normal epithelial cells in the gastric mucosa, gastrin and the CCK_2-R have been implicated in the pathogenesis of gastric adenocarcinomas (*7*−*9*).

The human CCK_1 and CCK_2 receptor subtypes share over 50% sequence identity and display equally high affinity for the sulfated forms of the multimeric family of carboxyamidated cholecystokinin peptides (e.g., CCK-58, CCK-33, and CCK-8). The CCK_2 receptor is less selective than CCK_1-R with respect to affinity for endogenous ligands and displays high affinity for gastrin and nonsulfated CCK (*6*). Identification of the determinants for the differences in ligand affinity, despite the high sequence homology, is an area of active research and one goal of the present study.

Indirect structural insight into the localization and nature of the agonist, antagonist, and G-protein binding sites in the CCK_2-R has been obtained through site-directed mutagenesis (*10*−*17*), chimera swap (*18*−*20*), N-terminal truncation (*21*), and photoaffinity labeling (*22*) studies. From these efforts, a number of residues in the N-terminus, extracellular loop 1 (EC1), EC2, and TM7 have been shown to alter the binding affinity of CCK to CCK_2-R. Far fewer direct intermolecular contact points between CCK_2-R and ligand have been identified (*22*, *23*). An interaction between $H207^2$ in EC2 of CCK_2-R and Asp^{32} was shown using a combination of site-directed mutagenesis and alanine scanning of CCK-9 (*23*). An N-terminal *p*-benzoylbenzoyl photoreactive probe of CCK-8 was observed to cross-link to the N-terminal TM1 region of CCK_2-R(L^{52}ELAIRITLY^{61}) (*22*). Ligand/receptor interactions involving TM6 and the EC3 of CCK_2-R have not been reported. This is in contrast with findings from the CCK_1-R, for which site-directed mutagenesis and photoaffinity labeling studies have identified intermolecular contact points between CCK and both TM6 (*24*) and EC3 (*25*).

Recently, the structure of the N-terminus, CCK_1-R(1−47) (*26*), and EC3, CCK_1-R(329−357) (*27*), domains of the

[†] This work was supported by the Research Foundation through a Cottrell Scholars Award (D.F.M.) and a Henry and Camille Dreyfus Scholars and Teachers Award (D.F.M.).

[‡] The structure coordinates have been deposited in the Brookhaven Protein Data Bank (filename 1L4T).

* To whom correspondence should be addressed at the Department of Molecular Pharmacology. Phone: (401) 863-2139. Fax: (401) 863-1595. E-mail: Dale_Mierke@Brown.edu.

[§] Department of Chemistry.

[||] Department of Molecular Pharmacology.

[1] Abbreviations: CCK, cholecystokinin; CCK_1-R, cholecystokinin type 1 receptor; CCK_2-R, cholecystokinin type 2 receptor; DG, distance geometry; DPC, dodecylphosphocholine; EC, extracellular loop; G-protein, guanine nucleotide-binding regulatory protein; MD, molecular dynamics; NMR, nuclear magnetic resonance; NOE, nuclear Overhauser enhancement; NOESY, nuclear Overhauser enhancement spectroscopy; RMSD, root-mean-square deviation; TM, transmembrane; TOCSY, total correlation spectroscopy.

[2] To simplify the description of the interaction in the ligand/receptor complex, the amino acids of the ligand will be denoted using the three-letter code, while the one letter code will be used for the residues of the receptor.

10.1021/bi0160009 CCC: $22.00 © 2002 American Chemical Society
Published on Web 03/15/2002

human CCK_1-R and their respective molecular complexes with CCK-8 have been determined by NMR spectroscopy in the presence of DPC micelles. NOEs indicating short-range intermolecular interactions were observed between the N-terminal residues of CCK-8 and the N-terminus of CCK_1-R(1−47) and between the C-terminal residues of CCK-8 and the TM6 region of CCK_1-R(329−357). The localization of the NOE-derived contact points was generally in good agreement with those obtained from site-directed mutagenesis and photoinduced labeling studies.

In this study, the NMR-derived structure of the third extracellular loop of the CCK_2 receptor, CCK_2-R(352−379), and its intermolecular interactions with CCK-8 are presented. A molecular model of the full receptor, based on the experimentally determined structure of EC3 and the NOE-derived intermolecular contact points, was used to delineate noncovalent interactions that stabilize the ligand−receptor complex. Molecular models of the CCK_1 and CCK_2 receptors are compared and contrasted to rationalize the observed differences in the ligand binding modes which may be related to the observed specificity of the receptor subtypes.

EXPERIMENTAL PROCEDURES

Peptide Synthesis. The receptor fragment CCK_2-R(352−379) was synthesized using solid-phase techniques at the Protein Chemistry Facility at Tufts University (Boston, MA). The receptor fragment was purified by semipreparative reverse-phase high-performance liquid chromatography, and the structural integrity was verified by mass spectrometry and NMR. CCK-8 ($D^{26}YMGWMDF^{33}$-NH_2) was purchased from Phoenix Pharmaceutics Inc. (Mountain View, CA; purity ≥95%).

NMR Methods. Peptide solutions were prepared in 50 mM phosphate buffer (90% H_2O/10% D_2O, Cambridge Isotopes) at a concentration of 1 mM peptide and 150 mM DPC-d_{38} (98.6%, Cambridge Isotopes). The final pH of the aqueous solution was 5.2 without correction for the deuterium isotope effect. Proton NMR spectra were recorded on a Bruker Avance 600 MHz spectrometer and processed using NMRPipe (*28*). NOE cross-peaks were integrated using Sparky (*29*).

TOCSY (*30*, *31*) and NOESY (*32*, *33*) spectra were recorded in the phase-sensitive mode using the method from States (*34*) at 298−308 K with mixing times of 50 and 150−300 ms, respectively. The WATERGATE pulse sequence was used for solvent suppression (*35*). The spectral width was 7500 Hz in both dimensions, with 2048 data points in f_2 and 640 data points in f_1, and 4−48 scans were collected at each increment.

The isolated two-spin approximation was used to convert NOESY cross-peak volumes into distances. Geminal cross-peaks between the β- and δ-methylene protons of F358 and P371, respectively, were used as an internal reference (1.8 Å). NOEs that could not be accurately integrated were assigned to three classes on the basis of intensity: strong, 1.8−3.0 Å; medium, 1.8−4.0 Å; and weak, 1.8−5.0 Å. For protons that could not be stereospecifically assigned, the upper distance restraints were corrected using standard procedures (*36*).

Structure Refinement. The structure of CCK_2-R(352−379) was determined by the random metrization, distance geometry (DG) algorithm of Havel (*37*) and the holonomic and experimentally determined distance restraints. Structures were initially embedded in four dimensions and refined following published procedures (*38*, *39*). The resulting structures were then reduced to three dimensions using metrization, and the optimization was repeated.

Molecular Dynamics of CCK_2-R(352−379). Molecular dynamics (MD) simulations of CCK_2-R(352−379) were performed using GROMACS v2.0 (*40*). A representative, low-energy DG structure was placed in the center of a water−decane solvent box ($x = y = z = 60$ Å). Amino acid side chains with ionizable functional groups at physiological pH (pH 7.4) were treated as charged species. During the MD simulation, the receptor fragment was subjected to an NOE-restrained simulated annealing protocol (800−300 K over 500 ps), followed by an NOE-restrained MD simulation at 300 K for 300 ps. A 10 Å cutoff distance was used for Coulombic and nonbonded interactions, and the neighbor list for nonbonded interactions was updated every 10 fs with a time step of 1 fs. A force constant of 5000 kJ mol^{-1} nm^{-2} was applied to the distance restraints throughout the entire simulation.

Molecular Modeling of the CCK_2 Receptor. A hydrophobicity plot of the amino acid sequence of CCK_2-R was used to identify long stretches of hydrophobic residues that could potentially constitute the TM domains of the receptor (*41*−*43*). The location of the TM domains was further refined by comparison to the amino acid sequence of other GPCRs (*44*, *45*) and by taking the helix-breaking propensities of the amino acid residues into account (*46*). The initial positions of the α carbons in the TM helices were template forced to the crystal structure of bovine rhodopsin (*47*) and then subjected to extensive dihedral angle-restrained steepest descent and conjugate gradient energy minimization. If necessary, the TM helices were rotated to satisfy the physicochemical properties of the amino acid side chains (*48*).

The experimentally determined structure of CCK_2-R(352−379) was incorporated into the model of the full receptor by template forcing the N- and C-termini to TM6 and TM7 of the CCK_2-R model. The experimentally determined structural features of the N-terminus of CCK_1-R(1−47) (*26*) were incorporated into homologous regions of the N-terminal region of the CCK_2-R (i.e., a disulfide bond between C22 and C39 and an amphiphilic helix between M1 and E11). To further restrain the extracellular domains of the receptor, the first and second extracellular loops were connected by a disulfide bond between C157 and C205, as described for other GPCRs (*47*, *49*−*51*). The entire receptor was subjected to NOE and dihedral angle-restrained energy minimization using steepest descent and conjugate gradients followed by template forcing of the TM helices to their initial positions observed in the X-ray structure of rhodopsin. Following the procedures previously described for CCK_1-R (*27*), the model of CCK_2-R was subjected to dihedral angle and NOE restrained MD simulations in a water−decane−water solvent box that mimicked the membrane environment of GPCRs.

RESULTS

Structure of CCK_2-R(352−379). The receptor fragment selected for this study corresponded to the entire putative third extracellular loop and several anchoring residues from

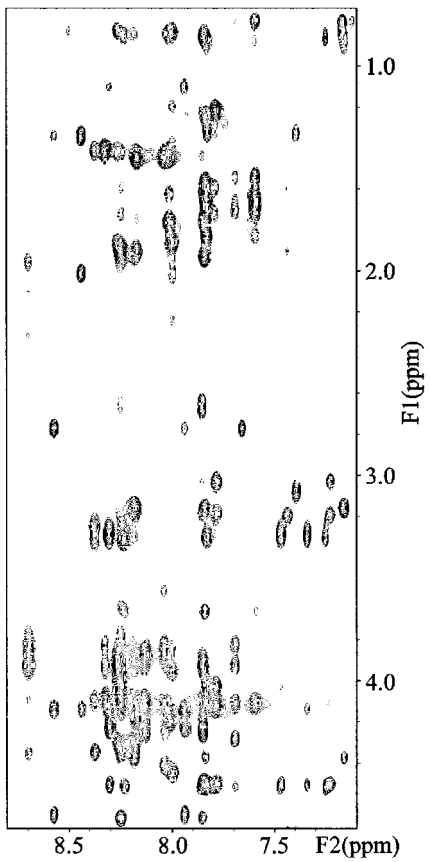

FIGURE 1: Expanded portion of a two-dimensional NOESY spectrum of CCK_2-R(352−379) collected at 298 K with a mixing time of 150 ms.

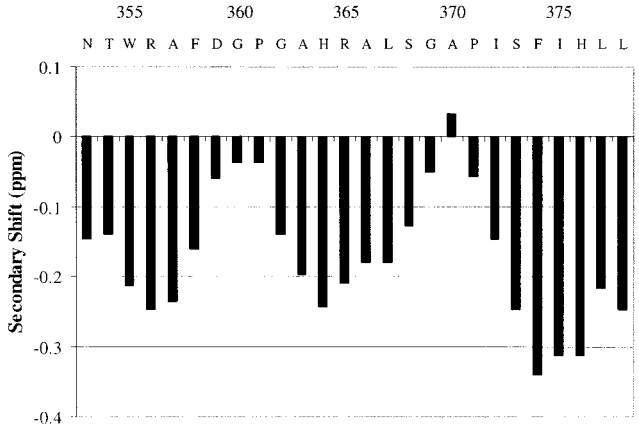

FIGURE 2: Hα secondary shifts for CCK_2-R(352−379). The chemical shifts were measured relative to TSP from a TOCSY spectrum collected at 35 °C with a mixing time of 50 ms.

the adjoining sixth and seventh transmembrane domains. Despite two proline residues, P361 and P371, only a single set of NMR signals was observed; $H^{\alpha}_i/H^{\delta}_{i+1}$ cross-peaks between the proline and the preceding residue indicate that these amide bonds are trans.

From the NOESY spectra collected at 298 and 308 K, a total of 318 unique distance restraints were generated and included throughout the structure refinement process (Figure 1). The chemical shift index of the Cα protons, shown in Figure 2, and many of the structurally important NOEs, provided in Figure 3, were consistent with the presence of helical elements in the N-terminal region between residues A352 and A357, in the extracellular loop region between A363 and S368, and in the C-terminal region between I372 and S379.

The structure refinement of CCK_2-R(352−379) was carried out using a two-step approach that included metric matrix DG calculations followed by MD simulations. The DG calculations generated structures satisfying the van der Waals contacts, chiral and planarity volumes, and the holonomic and experimental distance restraints without regard for energetically important intramolecular interactions (e.g., partial charges, Coulombic and Lennard-Jones interactions). Among the 91 DG structures generated, the individual distance violations were less than 0.23 Å, and the average pairwise RMSD of the backbone atoms was 0.76 Å. The ϕ/ψ dihedral angles of N353−A357, H364−L367, and I372−L378 formed tight clusters in the α-helical region (Figure 4). On the basis of ϕ/ψ dihedral angles, the residues between the helical regions, connecting the central, extracellular helix to the helical TM domains, were much less well structurally defined.

Structures from the DG calculations, representative of the ϕ/ψ pairs of the entire ensemble, were selected for a series of NOE-restrained MD simulations. To model the water−micelle environment, MD simulations of the receptor fragment were conducted in a two-phase solvent box composed of water and decane. The receptor fragment was positioned at the interface in accordance with the relative hydrophobicity of the amino acid side chains. In this initial configuration the N- (TM6) and C-terminal (TM7) helices were partially embedded in the decane phase, while the amino acid residues of the extracellular loop were aligned along the water−decane interface. During the course of the MD simulation, the C-terminal helix (TM7) became increasingly embedded in the decane phase, while the amphiphilic N-terminal (TM6) and extracellular loop helices were closely associated with the water−decane interface (Figure 4). The three helices identified in the DG structures were maintained throughout the entire MD simulation. During the last 50 ps of the simulation, the mean ϕ and ψ dihedral angles of T354−R356, H364−A366, and I372−L378 were consistent with an α-helix. At each time step of the simulation the mean distance violation was less than 0.2 Å.

CCK_2-R(352−379)/CCK-8 Complex. Intermolecular interactions between CCK-8 and CCK_2-R(352−379) were determined through the measurement of intermolecular NOEs and amide−proton chemical shift perturbations. The solubility of the ligand was limited to an effective concentration of ∼0.6 mM, as estimated by the relative intensities of the indole NH resonances of Trp^{30} and W355, respectively. Intermolecular NOEs were localized in the C-terminal region (TM7) of the receptor fragment between the amide proton of Met^{31} and the methylene protons of F374 and between the HE3 aromatic proton of Trp^{30} and the γ-protons of P371. In addition, concentration-dependent chemical shift perturbations were observed for the amide protons in a number of residues in the third extracellular loop and C-terminal (TM7) regions of the receptor fragment (Figure 5).

To determine the intermolecular interactions that contributed to the stability of the CCK-8/CCK_2-R(352−379) complex, a series of short (50 ps) MD simulations were carried out. The restraints used during these simulations consisted of the intramolecular NOEs for CCK_2-R(352−379)

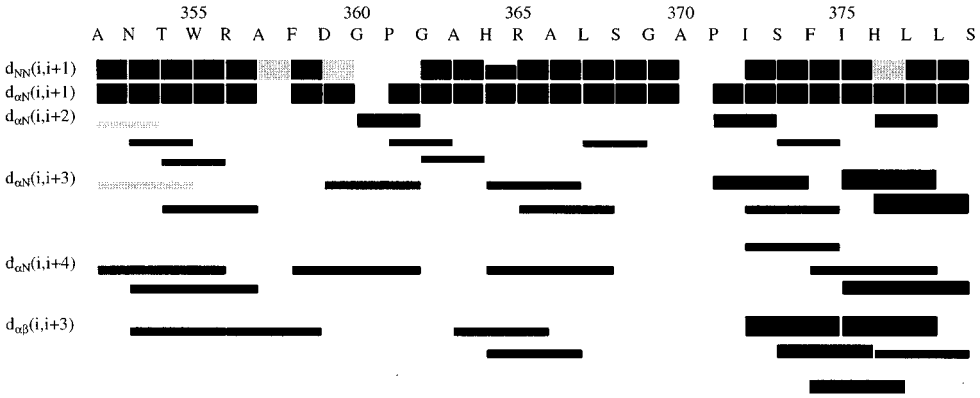

FIGURE 3: Structurally informative NOEs from NOESY spectra collected at 298 and 308 K. The NOEs were classified as strong, medium, and weak according to the intensity of the integrated cross-peak volumes. Partially overlapped cross-peaks are depicted with shaded bars.

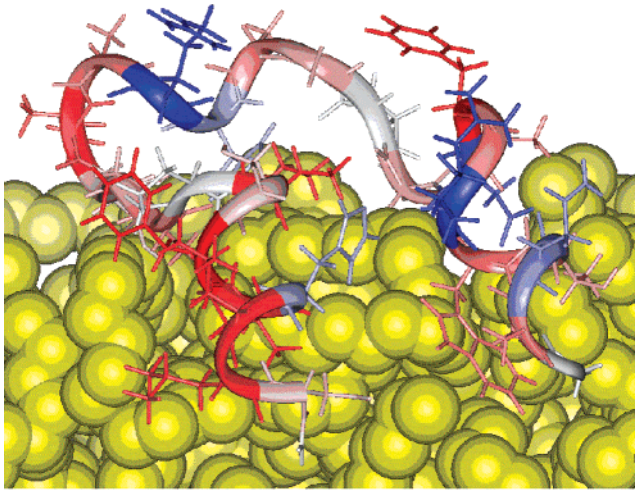

FIGURE 4: Structure of CCK$_2$-R(352−379) following an NOE-restrained MD simulation for 300 ps in a water−decane membrane mimetic solvent box with periodic boundary conditions. The amino acids of the receptor fragment are color coded according to hydrophobicity (blue = polar, red = hydrophobic), with TM7 and TM6 depicted on the left and right, respectively. The decane phase is depicted in gold CPK, and the water phase has been omitted for clarity.

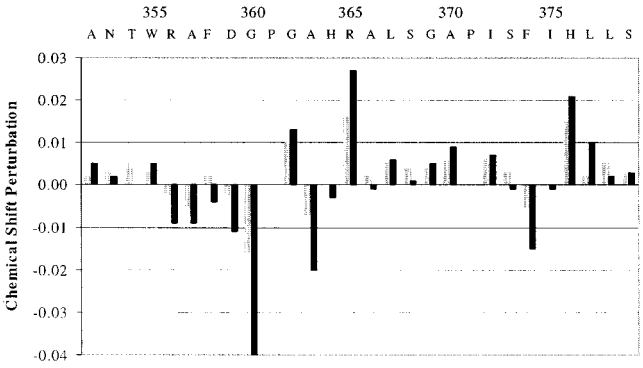

FIGURE 5: Amide proton chemical shift perturbations observed upon titration of CCK-8 to the CCK$_2$-R(352−379) receptor fragment.

and CCK-8 (*26*) and the intermolecular NOEs observed between the ligand and the receptor fragment. In the initial MD simulations of the complex, the intermolecular and intramolecular NOEs were used as restraints to "dock" the ligand from a position 10 Å removed from the receptor fragment. Each of the simulations differed from one another by the relative orientation of the ligand with respect to the receptor fragment. With the exception of simulations that lead to high-energy interactions (i.e., large distance violations and distorted structures), each of the simulations converged to a similar low-energy complex that was consistent with the applied distance restraints. The lowest energy configuration placed the pseudohelix of CCK-8 nearly perpendicular to the C-terminal helix (TM7) of the receptor fragment, with the C-terminal Phe^{33} residue directed toward the N-terminal helix (TM 6). The side chains of the Trp^{30}, Met^{31}, and Phe^{33} residues of the ligand were observed to intercalate in a hydrophobic pocket formed by the side chains of the P371, S373, F374, L377, and L378 residues in the C-terminal helix (TM7) of the receptor fragment.

On the basis of the chemical shift perturbations, an additional distance restraint was added to probe the effect of an electrostatic interaction between the carboxylic acid and guanidine functional groups of Asp^{32} and R365, respectively, on the binding orientation of the ligand. During the time course of the simulation, the electrostatic restraint produced a nearly 90° change in the tilt angle of the pseudohelix axis but did not alter the hydrophobic interactions described above. The distance between the Cγ atom of Asp^{32} and the Nϵ atom of R365 decreased from 15 to 8 Å upon application of the distance restraint. We conclude that the intermolecular NOEs are not consistent with a Coulombic interaction between Asp^{32} of CCK-8 and R365 of CCK$_2$-R.

Experimentally Based Model of the CCK-8/CCK$_2$ Receptor Complex. A model of the entire CCK$_2$-R was constructed to probe the intermolecular interactions that contributed to the stability of the complex between CCK-8 and the CCK$_2$-R. The experimentally determined structure of the CCK$_2$-R(352−379) receptor fragment was incorporated into the TM6 and TM7 domains of the receptor with only minor modifications to the distance between the TM helices. A helix was observed between A363 and S368 throughout the time course of the simulation, and the extracellular loop helix was closely associated with the water−decane interface. In the transition regions between TM6 and the extracellular loop helix, the residues form a loop conformation, whereas in the transition region between the extracellular loop helix and TM7, the amino acid residues were in an extended conformation.

The intermolecular NOEs observed between CCK-8 and the receptor fragment CCK$_2$-R(352−379) were used to

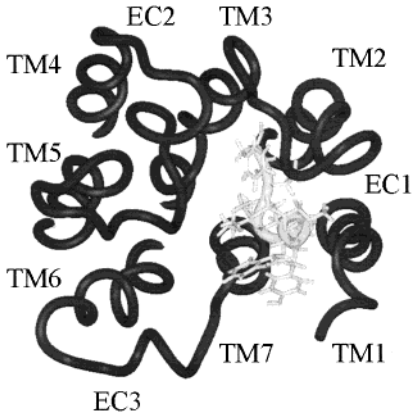

FIGURE 6: Top view of a molecular model of CCK_2-R and CCK-8 following 500 ps of NOE-restrained MD simulation in a membrane mimetic solvent box composed of a layer of decane sandwiched between two layers of water. For clarity, only the residues of the ligand are displayed.

Table 1: Notable Intermolecular Interactions between CCK-8 and CCK_2-R

ligand	receptor
Coulombic	
Asp^{32}	H207
hydrogen bonds	
Phe^{33} NH_2	F110 CO, T111 OH
Asp^{32} CO	H207 HE2
Asp^{32} CγO	N115 HN, NγH_2
Asp^{32} CγO	N115 HN, NγH_2, T111 OH, T119 OH
Tyr^{27} OH	R57 NH_2
hydrophobic	
Phe^{33}	P114, F120, I121, G123, I126
Met^{31}	T119, F120, W209, I372, F374
Trp^{30}	P371
Gly^{29}	I58

manually dock the ligand. During the simulation, the ligand adopted an orientation that placed its N-terminus near the N-terminus of the receptor, with the protonated amino terminus of Asp^{26} projecting into the aqueous phase (Figure 6). The C-terminus of the ligand was in close spatial proximity to TM2 and TM3, while the pseudohelix axis of CCK-8 was orientated at a 45° angle relative to the extracellular face of the TM bundle. A number of stabilizing intermolecular interactions between CCK-8 and the CCK_2-R were observed, as provided in Table 1.

DISCUSSION

The human CCK_1 and CCK_2 receptors share over 50% sequence identity, with the TM domains displaying the highest degree of sequence identity (66%), followed by the intracellular (37%) and extracellular (19%) domains. Most of the differences in the extracellular domains are located in the N-terminus, which plays a role in binding the longer forms of CCK (CCK-15) but is not required for the association of CCK-8 (*22*, *52*). The first extracellular loop, EC1, shown to be involved in ligand binding (*16*) is small (ca. six residues), limiting the possible structural features (particularly considering the 12 Å between the TM helices), and is very similar in CCK_1-R and CCK_2-R (67% identity). Therefore, to address the structural basis for the ligand specificity of CCK_1-R and CCK_2-R, we have concentrated our efforts on the third extracellular loop (EC3), implied in ligand binding to CCK_1-R by photoaffinity labeling and mutational analysis (*24*, *25*). The EC3 domain of CCK_2-R has 54% sequence identity with CCK_1-R.

In a previous study, we determined the structure of the EC3 of CCK_1-R, CCK_1-R(329−358), by high-resolution NMR in the zwitterionic environment of DPC micelles (*27*). The receptor domain contained three helical regions: A332−D339, A341−R346, and P351−L356. The overall conformational features of CCK_2-R(352−379) determined in this study are similar, with three helical regions observed between A351−A357 (extracellular portion of TM6), A363−S368 (EC), and I372−S379 (extracellular portion of TM7). Despite the similarity in overall structure, there are significant differences. In CCK_1-R(329−358), the transition between TM6 and the central helix occurs over two to three amino acids ($D^{339}TA^{341}$), whereas in CCK_2-R(352−379) the transition occurs over five to six amino acids ($F^{358}DGPGA^{363}$). This difference can largely be attributed to the helix-breaking propensities of the $G^{360}PG^{362}$ sequence in CCK_2-R(352−379). This produces a different topological orientation of the central helix in the two receptors; it is closer to TM6 in CCK_1-R and shifted toward TM7 in CCK_2. Additionally, the central helix, which is the same length in the two receptors, differs with respect to charged residues, CCK_1-R($E^{344}RR^{346}$) versus CCK_2-R($H^{364}RA^{366}$). The presence of the negatively charged residue, E344, in CCK_1-R plays an important role. During MD simulations, E344 interacts with R345, reducing its electrostatic potential for intermolecular interactions. Indeed, R345 of CCK_1-R can be mutated without much loss of CCK-8 binding (*53*). The MD simulations also indicate that the E344 of CCK_1-R forms a salt bridge with R336 in TM6, causing R336 to reorient, and project toward the TM bundle, in proximity to TM7 and the N-terminus of the receptor. An energetically favorable electrostatic interaction between Asp^{32} of CCK-8 and R336 of CCK_1-R has been identified by reciprocal mutations (*54*). In the absence of the negatively charged residue in EC3 of CCK_2-R, the corresponding residue in TM6, R356, would not be attracted to EC3, and instead there would be a repulsive interaction between R356 and R365. Although the general structural features of EC3 of CCK_1-R and CCK_2-R are similar, important differences in relative topology and electrostatics are observed. These observations, consistent with the available biochemical data, imply an alternative binding mode for the two receptor subtypes.

The NMR experiments on the interactions of CCK-8 and the TM6-EC3-TM7 domains of CCK_1-R and CCK_2-R provide experimental evidence for alternative binding modes. Specifically, for CCK_1-R(329−358), ligand/receptor NOEs involve residues in TM6 (N333, A334, and Y338) while for CCK_2-R(352−379), the contact points are localized in TM7 (P371 and F374). These results are consistent with a lateral translation of the pseudohelix of CCK-8 to a position closer to the proximal N-terminus and TM helices 1, 2, and 7, as compared to CCK_1-R. The result is that a majority of the ligand/receptor interactions in CCK_2-R involve the C-terminal tetrapeptide of CCK-8; in contrast, for CCK_1-R a number of interactions involving the N-terminus of the ligand (Asp^{26}, Tyr^{27}) have been identified (*26*, *54*, *55*). These observations are consistent with the preferential binding of CCK-4 to CCK_2-R over CCK_1-R.

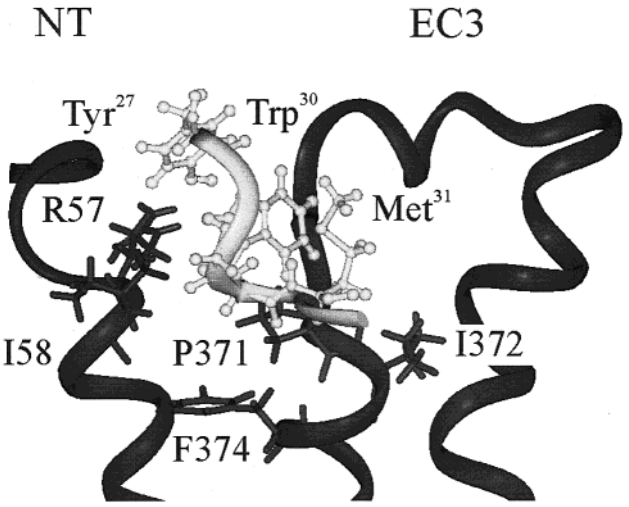

FIGURE 7: Side view of the extracellular portion of TMs 1, 6, and 7 in the molecular model of the CCK-8/CCK_2-R molecular complex. The side chains contributing to the complex are depicted in stick (receptor) and ball-and-stick (ligand) representation. The residues of the receptor and ligand are denoted by one and three letter codes, respectively.

Extensive NOE-restrained MD simulations of the CCK_2-R/CCK-8 complex, incorporating the structural features of EC3, suggest important roles for a number of residues of the receptor for ligand binding (Figure 7). Several of these amino acids have been shown to alter CCK-8 binding. Alanine-scanning mutagenesis of residues in the amino terminus and EC1 of CCK_2-R indicated that R57 in the top of TM1 and N115, L116, F120, and F122 in EC1 are important for maintaining high-affinity binding of CCK-8 (*16*). N-Terminal truncation studies (*21*) and, more recently, photoaffinity labeling (*22*) provide further support for interactions between the proximal N-terminus of CCK_2-R and the N-terminus of CCK-8 (or longer CCK ligands). A specific interaction has been identified between H207 of EC2 and Asp^{32} of CCK-9 (*16*). A single point mutation in the extracellular portion of TM7, H376L, results in a 29-fold drop in CCK-8 affinity (*12*). Although the NMR of the ligand/receptor complex in the present study does not show direct interactions between H376 and CCK-8, the adjacent residue F374 is directly involved in intermolecular NOEs with the ligand. This mutation was the most significant of a sequential replacement of the 58 nonconserved residues in the TM region of human CCK_2-R with the corresponding residues of CCK_1-R (*12*). Our findings are in accord with these results.

In summary, the conformational features of CCK_2-R(352−379) and its intermolecular interactions with CCK-8 were determined by high-resolution NMR in a membrane mimetic solvent system composed of DPC micelles. The observed intramolecular and intermolecular NOEs were used as restraints to model the interactions that contribute to the stability of the CCK-8/CCK_2-R complex. NOE-restrained MD simulations indicate that multiple intermolecular interactions involving residues at the membrane interface contribute to the stability of the complex. The interaction points, identified by intermolecular NOEs to be in the extracellular end of TM7, differ from those observed for the CCK-8/CCK_1-R(329−357) complex. When considered in the context of the full receptor/ligand model and the available biochemical data, these results suggest an alternative mode of binding for CCK-8 to CCK_1-R and CCK_2-R.

REFERENCES

1. Silvente-Poirot, S., Dufresne, M., Vaysse, N., and Fourmy, D. (1993) *Eur. J. Biochem. 215*, 513−529.
2. Wank, S. A. (1995) *Am. J. Physiol. 269*, G628−646.
3. Wank, S. A. (1998) *Am. J. Physiol. 274*, G607−613.
4. Dunlop, J. (1998) *Gen. Pharmacol. 31*, 519−524.
5. Noble, F., Wank, S. A., Crawley, J. N., Bradwejn, J., Seroogy, K. B., Hamon, M., and Roques, B. P. (1999) *Pharmacol. Rev. 51*, 745−781.
6. Noble, F., and Roques, B. P. (1999) *Prog. Neurobiol. 58*, 349−379.
7. Rehfeld, J. F., and van Solinge, W. W. (1994) *Adv. Cancer Res. 63*, 295−347.
8. Smith, A. M., and Watson, S. A. (2000) *Gut 47*, 820−824.
9. Henwood, M., Clarke, P. A., Smith, A. M., and Watson, S. A. (2001) *Br. J. Surg. 88*, 564−568.
10. Beinborn, M., Lee, Y. M., McBride, E. W., Quinn, S. M., and Kopin, A. S. (1993) *Nature 362*, 348−350.
11. Jagerschmidt, A., Guillaume, N., Goudreau, N., Maigret, B., and Roques, B. P. (1995) *Mol. Pharmacol. 48*, 783−789.
12. Kopin, A. S., McBride, E. W., Quinn, S. M., Kolakowski, L. F., Jr., and Beinborn, M. (1995) *J. Biol. Chem. 270*, 5019−5023.
13. Jagerschmidt, A., Guillaume-Rousselet, N., Vikland, M. L., Goudreau, N., Maigret, B., and Roques, B. P. (1996) *Eur. J. Pharmacol. 296*, 97−106.
14. Wang, H. L. (1997) *J. Neurochem. 68*, 1728−1735.
15. Jagerschmidt, A., Guillaume, N., Roques, B. P., and Noble, F. (1998) *Mol. Pharmacol. 53*, 878−885.
16. Silvente-Poirot, S., Escrieut, C., and Wank, S. A. (1998) *Mol. Pharmacol. 54*, 364−371.
17. Gales, C., Kowalski-Chauvel, A., Dufour, M. N., Seva, C., Moroder, L., Pradayrol, L., Vaysse, N., Fourmy, D., and Silvente-Poirot, S. (2000) *J. Biol. Chem. 275*, 17321−17327.
18. Mantamadiotis, T., and Baldwin, G. S. (1994) *Biochem. Biophys. Res. Commun. 201*, 1382−1389.
19. Silvente-Poirot, S., and Wank, S. A. (1996) *J. Biol. Chem. 271*, 14698−14706.
20. Schmitz, F., Pratt, D. S., Wu, M. J., Kolakowski, L. F., Jr., Beinborn, M., and Kopin, A. S. (1996) *Mol. Pharmacol. 50*, 436−441.
21. Miyake, A. (1995) *Biochem. Biophys. Res. Commun. 208*, 230−237.
22. Anders, J., Bluggel, M., Meyer, H. E., Kuhne, R., ter Laak, A. M., Kojro, E., and Fahrenholz, F. (1999) *Biochemistry 38*, 6043−6055.
23. Gigoux, V., Maigret, B., Escrieut, C., Silvente-Poirot, S., Bouisson, M., Fehrentz, J. A., Moroder, L., Gully, D., Martinez, J., Vaysse, N., and Fourmy, A. D. (1999) *Protein Sci. 8*, 2347−2354.
24. Gigoux, V., Escrieut, C., Fehrentz, J. A., Poirot, S., Maigret, B., Moroder, L., Gully, D., Martinez, J., Vaysse, N., and Fourmy, D. (1999) *J. Biol. Chem. 274*, 20457−20464.
25. Hadac, E. M., Pinon, D. I., Ji, Z., Holicky, E. L., Henne, R. M., Lybrand, T. P., and Miller, L. J. (1998) *J. Biol. Chem. 273*, 12988−12993.
26. Pellegrini, M., and Mierke, D. F. (1999) *Biochemistry 38*, 14775−14783.
27. Giragossian, C., and Mierke, D. F. (2001) *Biochemistry 40*, 3804.
28. Delaglio, F., Grzesiek, S., Vuister, G. W., Zhu, G., Pfeifer, J., and Bax, A. (1995) *J. Biomol. NMR 6*, 277−293.
29. Goddard, T. D., and Kneller, D. G. (2001) University of California, San Francisco.
30. Braunschweiler, L., and Ernst, R. R. (1983) *J. Magn. Reson. 53*, 521−528.
31. Bax, A., and Davis, D. G. (1985) *J. Magn. Reson. 65*, 355−360.
32. Macura, S., Huang, Y., Suter, D., and Ernst, R. R. (1981) *J. Magn. Reson. 43*, 259−281.

33. Jeener, J., Meier, B. H., Bachmann, P., and Ernst, R. R. (1979) *J. Chem. Phys. 71*, 4546−4553.
34. States, D. J., Haberkorn, R. A., and Ruben, D. J. (1982) *J. Magn. Reson. 48*, 286−292.
35. Piotto, M., Saudek, V., and Sklenar, V. (1992) *J. Biomol. NMR 2*, 661−665.
36. Wuthrich, K., Billeter, M., and Braun, W. (1983) *J. Mol. Biol. 169*, 949−961.
37. Havel, T. F. (1991) *Prog. Biophys. Mol. Biol. 56*, 43−78.
38. Mierke, D. F., Scheek, R. M., and Kessler, H. (1994) *Biopolymers 34*, 559−563.
39. Pellegrini, M., Gobbo, M., Rocchi, R., Peggion, E., Mammi, S., and Mierke, D. F. (1996) *Biopolymers 40*, 561−569.
40. Berendsen, H. J. C., van der Spoel, D., and van Buuren, R. (1995) *Comput. Phys. Commun. 95*, 43−56.
41. Eisenberg, D., Weiss, R. M., and Terwilliger, T. C. (1982) *Nature 299*, 371−374.
42. Eisenberg, D., Schwarz, E., Komaromy, M., and Wall, R. (1984) *J. Mol. Biol. 179*, 125−142.
43. Kyte, J., and Doolittle, R. F. (1982) *J. Mol. Biol. 157*, 105−132.
44. Baldwin, J. M. (1993) *EMBO J. 12*, 1693−1703.
45. Baldwin, J. M., Schertler, G. F., and Unger, V. M. (1997) *J. Mol. Biol. 272*, 144−164.
46. Chou, P. Y., and Fasman, G. D. (1978) *Annu. Rev. Biochem. 47*, 251−276.
47. Palczewski, K., Kumasaka, T., Hori, T., Behnke, C. A., Motoshima, H., Fox, B. A., Le Trong, I., Teller, D. C., Okada, T., Stenkamp, R. E., Yamamoto, M., and Miyano, M. (2000) *Science 289*, 739−745.
48. Donnelly, D., Overington, J. P., and Blundell, T. L. (1994) *Protein Eng. 7*, 645−653.
49. Karnik, S. S., and Khorana, H. G. (1990) *J. Biol. Chem. 265*, 17520−17524.
50. Noda, K., Saad, Y., Graham, R. M., and Karnik, S. S. (1994) *J. Biol. Chem. 269*, 6743−6752.
51. Cook, J. V., and Eidne, K. A. (1997) *Endocrinology 138*, 2800−2806.
52. Kennedy, K., Escrieut, C., Dufresne, M., Clerc, P., Vaysse, N., and Fourmy, D. (1995) *Biochem. Biophys. Res. Commun. 213*, 845−852.
53. Gouldson, P., Legoux, P., Carillon, C., Dumont, X., Le Fur, G., Ferrara, P., and Shire, D. (2000) *Eur. J. Pharmacol. 389*, 115−124.
54. Kennedy, K., Gigoux, V., Escrieut, C., Maigret, B., Martinez, J., Moroder, L., Frehel, D., Gully, D., Vaysse, N., and Fourmy, D. (1997) *J. Biol. Chem. 272*, 2920−2926.
55. Ding, X. Q., Dolu, V. V., Hadac, E. M., Holicky, E. L., Pinon, D. I., Lybrand, T. P., and Miller, L. J. (2001) *J. Biol. Chem. 276*, 4236−4244.

BI0160009